Gigahertz optoacoustic imaging for cellular imaging

Min Rui[a], Sankar Narashimhan[a], Wolfgang Bost[b], Frank Stracke[b], Eike Weiss[c], Robert Lemor[b], Michael C. Kolios*[a]
[a]Department of Physics, Ryerson University, Toronto, Canada;
[b]Fraunhofer Institute of Biomedical Engineering, St. Ingbert, Germany
[c]Kibero GmbH, Saarbrucken, Germany

ABSTRACT

Photoacoustic imaging exploits contrast mechanisms that depend on optical and thermomechanical properties of optical absorbers. The photoacoustic signal bandwidth is dictated by the absorber size and the laser pulse width. In this work we demonstrate that photoacoustic signals can be detected from micron and sub-micron particles. We anticipate applications to include cellular imaging with nanometer sized contrast agents such as gold nanoshells, nanorods, and nanocages.

An existing acoustic microscopy system was used (the SASAM 1000, kibero GmbH). This platform is developed on an Olympus IX81 optical microscope with a rotating column that has an optical condenser for transmission optical microscopy and an acoustic module for the acoustic microscopy. The adapted optoacoustic module consists of a Q-switched Nd:YAG solid-state-laser (Teem Photonics, France) generating sub-nanosecond pulses. Scans were acquired of microparticles (1 μm black Toner particles) and cells.

The confocal arrangement allowed high signal to noise ratio photoacoustic signals (>30 dB) to be detected at approximately 400 MHz. The particles of various sizes produced signals of different frequency content. In imaging mode, the full width half maximum (FWHM) was measured to be 3.6 μm for the 400 MHz transducer which is in general agreement theory for a 0.3 NA objective (4.3μm). Moreover, images are generated from single melanoma cells, generated by the endogenous contrast from the intracellular melanin.

.

Keywords: optoacoustic imaging, cellular imaging, nanotechnology, optoacoustic spectroscopy, ultrasound characterization.

1. INTRODUCTION

Optoacoustic imaging is a biomedical imaging modality that combines optical contrast with ultrasonic resolution [1]. Part of the interest in this imaging modality stems from the fact that the richness in contrast that has been developed in other optical techniques (such as fluorescent microscopy) can be exploited to make subsurface measurements that cannot be made with pure optical techniques. This is achieved by the production of broadband ultrasonic signals emanating from the locations of the optical energy absorption. Since ultrasound does not scatter in tissue as much as light, imaging depths of several centimeters can be achieved. Moreover, different optical excitation wavelengths can be used in order to produce signals from the chromophore of interest and therefore contrast mechanisms can be changed by the selection of the appropriate laser wavelength. In recent years, exquisite images of the human and small animal vasculature have been produced by exploiting the large optical absorption of oxygenated and de-oxygenated blood at the relevant optical wavelengths [2, 3]. In these images, individual capillaries can be resolved, and within those individual capillaries, single red blood cells can be detected. Since the resolution of the imaging modality depends on both the optical excitation method and ultrasound detection device, the question arises as to what resolution can be achieved by selecting the appropriate ultrasound bandwidth than optical excitation techniques. For example, if one wanted to image subcellular features, what laser pulse length and what ultrasound transducers should be used? This question is of increasing relevance now that it has been shown that fluorescent proteins can be used to generate optoacoustic signals, generating the intriguing possibility of using the fluorescent proteins as the absorbing structures of interest [4-6].

Theoretical calculations show that as long as the conditions of thermal and stress confinement are realized [7], the signals produced by a single spherical absorber have central ultrasonic frequencies that are dominated by two physical factors: a) the size of the absorbing object (and the speed of sound through the absorber) and b) the pulse length of the

Photons Plus Ultrasound: Imaging and Sensing 2010, edited by Alexander A. Oraevsky, Lihong V. Wang,
Proc. of SPIE Vol. 7564, 756411 · © 2010 SPIE · CCC code: 1605-7422/10/$18 · doi: 10.1117/12.841479

laser excitation [8, 9]. In Figure 1 theoretical simulation pressure profiles are plotted that demonstrate the transient pressures that are generated for spherical optical absorbers of a) 1 mm diameter and b) 1 μm diameter when an incident delta pulse of laser light is absorbed (assuming uniform absorption of light throughout the absorber). The bipolar pressure profile that is produced by the spherical absorber has a width that is related to the size of the absorbing object and is on the order of 1 μs for the 1 mm diameter absorber and 1 ns for the 1 μm diameter absorber. While the profiles in Figure 1 are generated by an instantaneous pulse, a pulse of finite width would involve convolving this profile with a Gaussian profile (assuming the time profile of the optical pulse is Gaussian), producing a smoother bipolar pulse. Even in this case, the peak to peak separation of the bipolar pulse, which determines the dominant frequency component of the signal, remains the same. Therefore, to optimally detect the signal generated by such absorbers, ultrasonic transducers that are sensitive to frequencies on the order of MHz are required for the millimeter diameter absorbers and transducers that are sensitive to frequencies on the order of GHz are required for the micrometer absorbers. Moreover, the shorter the laser pulse that is used to excite the absorbing structures, the more the pressure transients generated would be similar to the theoretically predicted profiles of Figure 1. A short laser pulse would also ensure that the smallest absorbing structures within the sample of interest also meet the conditions of stress and thermal confinement and therefore produce a photoacoustic signal that can be potentially detected with the appropriate transducer.

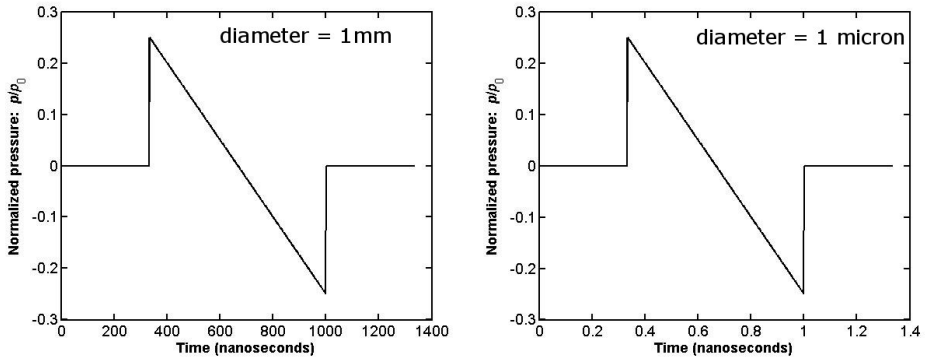

Figure 1: Theoretically predicted normalized pressure profiles, at a distance equal to 2 radii from the source, for a sphere of radius 1 mm (left panel) and 1 μm (right panel). The time between the two peaks of the bipolar pressure profile is of the order of microseconds for the 1 mm diameter sphere, and of the order of nanoseconds for the 1 μm sphere, corresponding to frequencies in the MHz and GHz range, respectively.

In this work, a modified scanning acoustic microscope is used to detect such pressure transients from micron sized objects. In the first part pressure profiles detected using 60, 205 and 375 MHz transducers are shown for micron sized ink particulates. In the second part, images of melanoma cells and red blood cells are generated to confirm that photoacoustic signals can be generated and detected at these frequencies. To the authors' best knowledge, these images are the first ever produced of photoacoustic signals detected from individual subcellular absorbers within a cell.

2. METHODS

The photoacoustic system used in this study has been described in previous publications. Briefly, a scanning acoustic microscope developed at the Fraunhofer Institute for Biomedical Technology (SASAM 1000, commercialized through Kibero GmbH, Saarbrücken, Germany) was modified to include a laser source, as described in [10]. The system consists of an inverted optical microscope (Olympus IX 81, Tokyo, Japan), a laser source, a single element transducer and the SASAM 1000 electronics module [11]. A focused pulsed laser is used to generate an optoacoustic signal The laser is a Q-switched Nd:YAG solid-state-laser (Teem Photonics, France) which is capable of producing sub-nanosecond micro-Joule pulses at kilohertz repetition rates. The solid state laser is coupled to the photoacoustic instrument via single mode fiber (core diameter 5 μm) and is focused on the sample using the microscope optics. Each pulse used in this experiment had a pulse energy of 350 nJ and a duration of 700 ps. Black toner particles with size of 1 μm were used as photoacoustic targets and imaged with various transducers working at centre frequencies of 60 MHz, 205 MHz and 375 MHz, confirming the photoacoustic signals generated for a large band of frequencies. The in-vitro experiments were performed with mouse melanoma cells (B16-F1) that were obtained from the American Type Culture Collection (ATCC, Rockville, MD, USA) and were grown in DMEM supplemented with 10%FBS (Invitrogen Canada Inc., Burlington, Ontario, Canada) at 37^0C in 5% CO2 under humidified conditions. The B16F1 cells were seeded in the Lab-Tek II

chambered cover glasses (Nunc, Thermo Fisher Scientific, Rochester, USA) 48 hours prior to an experiment. Before data acquisition, cells were fixed with 4% paraformaldehyde for 10 minutes at room temperature. Then cell medium was replaced with coupling medium: DMEM with 10% FBS plus 10 mM of MES solution (Sigma-Aldrich) to sustain the pH of cell medium. The chambered cover glass was transferred to the microscope at and was maintained at 37^{0}C during all measurements. For the portion of the experiment in which cells were imaged with multiple transducers, the cells were fixed to prevent cell motion as each photoacoustic scan would take a couple of minutes depending on the step size of the raster scan and the number of ultrasound signals averaged at each location. For the red blood cell experiments, sheep red blood cells (suspended at 10% in PBS) were purchased from Innovative Research (Michigan, USA).

3. RESULTS AND DISCUSSION

To illustrate the sensitivity and spatial resolution of the system, an ink particle was measured by the optoacoustic system. Figure 2 shows an optical image (left), photoacoustic image (middle) and a radio-frequency line taken from the center of the particulate (right). High signal to noise (SNR) photoacoustic signals were recorded for this optical absorber when using an ultrasound transducer whose sensitivity peaks at 375 MHz. As the measured signal is expected to be a convolution of signal generated from the absorbing particle (see figure 1), the laser pulse and the sensitivity pattern of the transducer, the measured profile does not have the simple bipolar shape predicted by theory. Taking the normalized amplitude profile of a line through the imaged 1 μm toner particle, a full width half maximum value of 3.6 μm is obtained, in line with the expectations for the 375 MHz transducer used in this experiment.

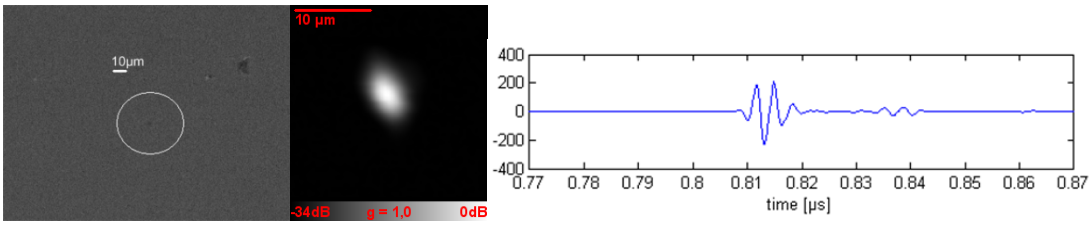

Figure 2: Photoacoustic image, collected with a 400 MHz transducer, of a ~ 1 μm ink particle. Microscopy image of the ink particulate (left) and photoacoustic image (middle) demonstrate the high resolution and good signal to noise of the system. The radiofrequency line is plotted in the far right.

The cell images are shown in figure 3. An optical image of a collection of melanoma cells is shown in panel (A) (the scalebar is 10 μm). Panels (B) and (C) depict photoacoustic images of these cells acquired using transducers with central frequencies of 205MHz and 375 MHz, respectively. Strong signals are detected from locations within the melanoma cells, and several of these features are sub-micron in size. Independent analysis confirms that the strongest of the signals are at locations where large melanin granules exist within the melanoma cells (e.g. location of yellow arrow). However, not every feature in the images has an obvious structural correlate in the optical microscopy. This may be due to the fact that the melanin granules that generate the photoacoustic signal cannot be detected/resolved with plain optical microscopy (limited contrast or the structure too small) or that other absorbing structures from within the cell contribute to this signal. We are in the process of indentifying these intracellular absorbing structures. Between the two images acquired at the different frequencies (panels B and C), there is a correlation between the location and general shape of the structures resolved. As expected, structures could be better resolved with the higher frequency transducer (e.g. the Y shape feature above yellow arrow in panel B). Moreover, the photoacoustic signal strength between the two images shows that some structures produce stronger signals when imaged with the 375 MHz transducer (yellow arrow), while others when imaged with the 205 MHz transducer (the Y structure above the arrow). Such a pattern has been observed with other cells (data not shown) and may be related to the absorbing structure size: smaller structures emit photoacoustic signals with higher frequency components that only higher frequency transducers would be able to detect with adequate sensitivity. Our laboratory is in the process of confirming this and is conducting experiments with well controlled bead sizes in the micrometer range. Finally, representative RF lines are shown from the data collected at the locations of the yellow arrows. The SNR of these measurements is high (>30dB), indicating that much lower laser outputs could be used to image the cells and that the strength of the photoacoustic signals detected at these frequencies is high. This is despite the fact that at these frequencies the ultrasound attenuation in the coupling medium is high: at room temperature, the attenuation of water at 200 MHz is ~ 88 dB/cm and at 1200 MHz the attenuation is 3165 ~ dB/cm (the distance between the cell and the transducer – focal distance- is approximately 500 μm for the 205 MHz transducer and

the 350 μm for the 375 MHz transducer). Since the ultrasound transducer is highly focused (and therefore has a geometrical gain) and the light spot size is in the order of a few micrometers, high sensitivity and resolution data from the cell can be collected. Features in the RF data presented are still being examined to ascertain their origin.

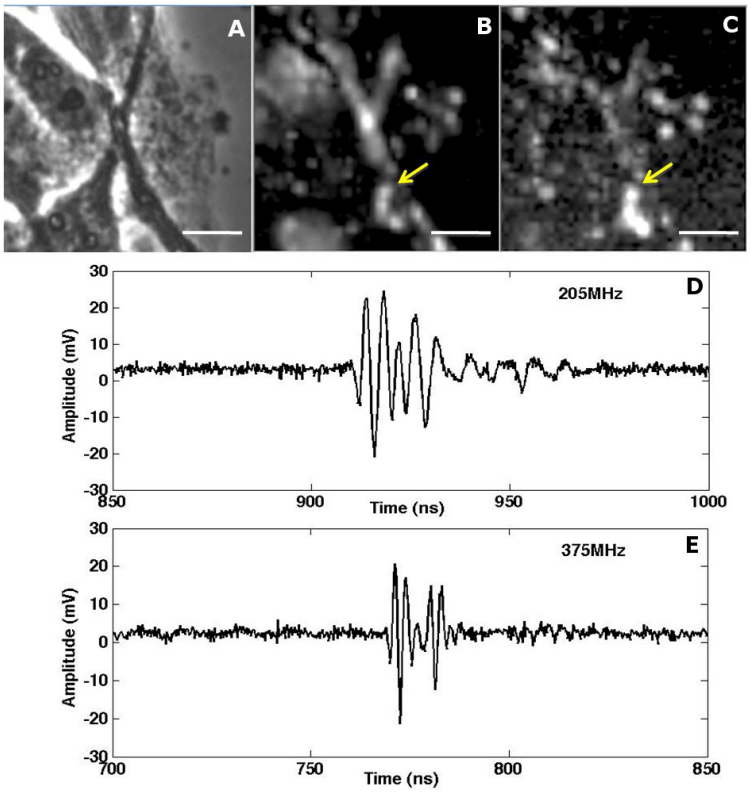

Figure 3: Mouse melanocyte B16F1 photoacoustic images. The B16F1 cells were cultured in the Lab-Tek II chambered cover glasses and fixed with 4% paraformaldehyde before imaging. Top panel shows B16F1 optical image (A) and photoacoustic C-scan images at central frequencies of 205MHz (B) and 375MHz (C). Single photoacoustic RF signals from the positions denoted by the arrow are displayed below (using the transducers with central frequencies of 205MHz and 375MHz, respectively). Scale bars are 10μm.

Similar experiments were performed with individual red blood cells, and strong signals were obtained for both of the ultrasound transducer frequencies. Even though red blood cells do not have their peak optical absorption at the laser wavelengths used (1064 nm), strong signals were detected as shown in figure 4. In panel A, an optical image of the red blood cell is shown and in panel B an optoacoustic image of the red blood cell is shown (the scale bar is 10 μm). The striations in the image are caused by motion of the red blood cell: the red blood cell is not immobilized on the substrate and the motion of the ultrasound transducer as it raster scans the region of interest itself creates the motion of the red blood cell during the imaging session. The RF data associated with a typical RBC is shown in panel C. Again, a strong SNR photoacoustic signal is recorded. Of particular interest is the power spectrum of the RF data. This is shown in panel D, for 10 separate power spectra derived from RF data of different red blood cells within the field of view of the instrumentation. In the same panel, the conventional ultrasound pulse echo reflection of the 375 MHz transducer (which is a representation of the sensitivity of the transducer) is shown on the same graph. It can be seen that the power spectra from all of the red blood cells examined have similar frequency power spectra, indicating uniformity in the size of the absorbing structure. Moreover, the shape of the power spectrum does not follow the exact shape of the transducer sensitivity pattern indicating that the cells themselves have a distinct power emission spectrum (that we assume is related to the size of a red blood cell). Therefore, in photoacoustic imaging, spectroscopy can be done in both the optical sense (by changing the laser wavelengths used to illuminate the sample) but also in the ultrasound sense (by examination of the frequency dependence of the pressure waves produced by the absorbing object). This is quite similar to the methodology that is applied in the field of ultrasonic tissue characterization[12-14], in which the frequency dependence of the

backscattered data is used to infer tissue microstructure since scatterers of different size modulate the frequency content of the backscattered wave[15]. A major difference however is that in photoacoustic imaging the size of the absorbing objects determine the frequency content of the pressure waves generated, irrespective of the transducer used to detect the signal, whereas in ultrasound imaging size of the object, in relation to the wavelength of the ultrasound pulse, determines the scattered wave frequency content. Therefore, in ultrasound imaging, one knows what detection ultrasound bandwidth to use, as it is similar to the interrogating ultrasound pulse bandwidth, but in photoacoustic imaging all the frequency components are present in the photoacoustic signals produced, and the ultrasound transducer bandwidth determines which features the measurements are most sensitive to. It is promising that such reproducible photoacoustic signals are produced when imaging a series of different red blood cells.

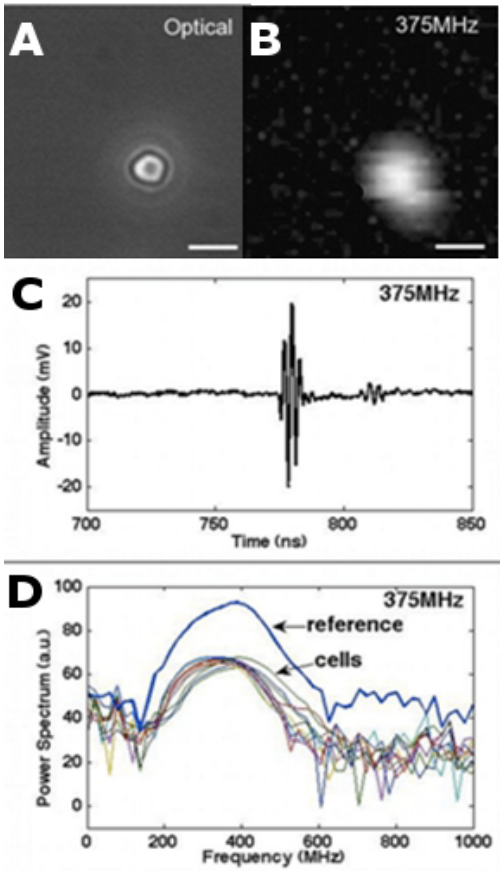

Figure 4: Optoacoutic image of a red blood cell. Panel A shows an optical image of a red blood cell. Panel B shows the corresponding optoacoustic image obtained with the 375 MHz transducer. A representative RF line is shown in panel C. Panel D shows the power spectrum from 10 different red blood cells (labeled cells and indicated by bottom arrow) and the pulse echo reference from the glass substrate (labeled reference and indicated by top arrow). Scale bars for panels A and B are 10 μm.

4. CONCLUSION

In this work, and for the first time to the our best knowledge, photoacoustic signals in the Gigahertz range are used to image cells based on endogenous absorbers within the cells. It was shown that photoacoustic signals are produced and detected by micron sized objects with high signal to noise ratios. Moreover, the feasibility of utilizing ultrasound spectroscopy, together with optical spectroscopy, for the characterization of biological materials and tissues is demonstrated. Future work will involve the elucidation of the absorption mechanisms for various cellular structures and well controlled experiments with absorbers of sub-micron size (including fluorescent micron sized beads and gold nanoparticles) to further demonstrate the potential of optoacoustic microscopy for the elucidation of absorbing structures.

This research was undertaken, in part, thanks to funding from the Canada Research Chairs Program awarded to Michael C. Kolios. Financial support for this study was provided by the Natural Sciences and Engineering Research Council of Canada and the Canada Foundation for Innovation (CFI).

REFERENCES

[1] L. V. Wang, "Prospects of photoacoustic tomography," Med Phys, 35(12), 5758-67 (2008).

[2] S. Hu, K. Maslov, and L. V. Wang, "Noninvasive label-free imaging of microhemodynamics by optical-resolution photoacoustic microscopy," Opt Express, 17(9), 7688-93 (2009).

[3] H. F. Zhang, K. Maslov, M. L. Li *et al.*, "In vivo volumetric imaging of subcutaneous microvasculature by photoacoustic microscopy," Opt Express, 14(20), 9317-23 (2006).

[4] R. Ma, A. Taruttis, V. Ntziachristos *et al.*, "Multispectral optoacoustic tomography (MSOT) scanner for whole-body small animal imaging," Opt Express, 17(24), 21414-26 (2009).

[5] D. Razansky, J. Baeten, and V. Ntziachristos, "Sensitivity of molecular target detection by multispectral optoacoustic tomography (MSOT)," Med Phys, 36(3), 939-45 (2009).

[6] D. Razansky, C. Vinegoni, and V. Ntziachristos, "Multispectral photoacoustic imaging of fluorochromes in small animals," Opt Lett, 32(19), 2891-3 (2007).

[7] A. A. Oraevsky, R. O. Esenaliev, S. L. Jacques *et al.*, "Laser optic-acoustic tomography for medical diagnostics: principles," Biomedical Sensing, Imaging, and Tracking Technologies I. 2676, 22-31.

[8] G. J. Diebold, M. I. Khan, and S. M. Park, "Photoacoustic "Signatures" of Particulate Matter: Optical Production of Acoustic Monopole Radiation," Science, 250(4977), 101-104 (1990).

[9] G. J. Diebold, T. Sun, and M. I. Khan, "Photoacoustic monopole radiation in one, two, and three dimensions," Phys Rev Lett, 67(24), 3384-3387 (1991).

[10] W. Bost, F. Stracke, E. C. Weiss *et al.*, "High frequency optoacoustic microscopy," Conf Proc IEEE Eng Med Biol Soc, 1, 5883-6 (2009).

[11] E. C. Weiss, P. Anastasiadis, G. Pilarczyk *et al.*, "Mechanical properties of single cells by high-frequency time-resolved acoustic microscopy," IEEE Trans Ultrason Ferroelectr Freq Control, 54(11), 2257-71 (2007).

[12] F. L. Lizzi, S. K. Alam, S. Mikaelian *et al.*, "On the statistics of ultrasonic spectral parameters," Ultrasound Med Biol, 32(11), 1671-85 (2006).

[13] F. L. Lizzi, M. Greenebaum, E. J. Feleppa *et al.*, "Theoretical framework for spectrum analysis in ultrasonic tissue characterization," J Acoust Soc Am, 73(4), 1366-73 (1983).

[14] M. F. Insana, and T. J. Hall, "Characterising the microstructure of random media using ultrasound," Phys Med Biol, 35(10), 1373-86 (1990).

[15] M. Kolios, "Biomedical ultrasound imaging from 1 to 1000 MHz," Canadian Acoustics - Acoustique Canadienne, 37(3), 35-43 (2009).